19th Brazilian Congress of Thermal Sciences and Engineering
November 06th-10th, 2022, Bento Gonçalves - RS - Brazil

ENC-2022-0056
REAL-TIME HEAT FLUX ESTIMATION IN TURNING PROCESS USING INVERSE PROBLEM TECHNIQUE AND INFRARED THERMOGRAPHY

Fernando Viana Avelar Dutra
Diego Corrêa Ferreira
Rodrigo Gustavo Dourado da Silva
Sandro Metrevelle Marcondes de Lima e Silva
Laboratório de Transferência de Calor – LabTC, Instituto de Engenharia Mecânica – IEM, Universidade Federal de Itajubá, Campus Prof. José Rodrigues Seabra, Av. BPS, 1303, Bairro Pinheirinho, Itajubá – MG, CEP 37500-903.
fernandovianadutra@unifei.edu.br
diegoc.ferreira@yahoo.com.br
rodrigogdourado@unifei.edu.br
metrevel@unifei.edu.br

Abstract. *The turning process is widely used in industry. Depending on the workpiece application some turning processes require tighter tolerances. These tolerances can be compromised by a considerable number of variables. The heat aspects are focused in this paper. Heat is generated on the tool-chip contact principally due to shear and frictional forces. This heat results in a large increase in temperature, which change properties of cutting tool and workpiece. Depending on the set-up of the process, the developed temperature could quickly lead to the breakage of the cutting tool. A program was developed for monitoring purpose. The program was able to estimate the heat flux and the hot spot temperature in real-time. It consists of solving an Inverse Heat Conduction Problem (IHCP) applying a filter coefficients technique. The function specification technique was used for the estimation of the filter coefficients. An infrared camera was used to measure the temperatures in accessible areas on the surface of a cutting tool. It was estimated a heat flux in the order of* 1.4×10^7 *W/m*^{2} *and a hot spot temperature reaching approximately 700 °C. This study is useful to support the development of practical tool wear monitoring systems and helps to exemplify the benefits of heat and temperature estimations.*

Keywords: *Inverse problem, heat flux, turning process, infrared thermography, real-time estimation*

1. INTRODUCTION

During machining, there is an intense mechanical work acting on the tool-chip contact area. Most of this mechanical work is converted into heat resulting in a large increase of temperature (Rezende et al., 2020). The temperature increase can damage and lead to the breakage of the cutting tool, impacting the accuracy of the machining process (Grzesik and Nieslony, 2003) and (Abukhshim et al., 2006). Although temperature monitoring is of fundamental interest in this phenomenon, measuring it at the tool-chip interface can be a challenging task due to presence of the chips and the small contact area (Le Coz et al., 2012) and (Valiorgue et al., 2013).

In an attempt to manage temperature measurements on the cutting region, researchers have been exploring many techniques like sensorial measurements as well as both analytical and numerical models (Arrazola et al., 2013). Additionally, the development of an on-line temperature monitoring systems is well seen as it induces better control of the process. Thus, some effects of high temperatures at the cutting edge could be monitored, resulting in a machining without such restricted cutting velocities, a larger tool life and workpieces with appropriate surface finishing (Abukhshim et al., 2005).

The direct use of the differential form of the energy conservation law is limited due to the unknown boundary conditions like the heat flux in the tool-chip contact interface. Therefore, the use of some inverse problem techniques is relevant. Beck and Woodbury (2016) used the tools provided by the scaled sensitivity coefficients, digital filter coefficients and intrinsic verification to compare several methods proposed to solve the Inverse Heat Conduction Problem (IHCP). Sheikh-Ahmad et al. (2019) employed an inverse heat conduction technique to determine the energy balance at the cutting zone in edge trimming of carbon fiber-reinforced polymer composites. The portions of heat going into the workpiece, tool and chips were respectively 0.07, 0.56 and 0.37.

Different measurement techniques were applied to support the thermal behavior study on tool-chip contact area. The cutting movement associated with the dimensions of the cutting tool, the small cutting area and the inherent constraints of the machining such as chip evacuation turn the precise positioning of thermocouples into a difficult task (Carvalho et al., 2006) and (Liang et al., 2013). Therefore, research has been employing infrared thermography to avoid measurement problems and facilitate temperature acquirement. Heigel et al. (2017) used an infrared (IR) camera to measure the temperature distribution on the tool–chip interface. Temperature distribution analysis from one edge of the chip to the other presented differences from 6% to 21%. Soler et al. (2018) presented a new method to measure the rake face temperature during dry orthogonal cutting using an infrared camera. Temperatures are directly measured without the need of emissivity correction.

Real time monitoring of tool wear is a key factor in the modern-day automated manufacturing for quality control of machined parts. Najafi and Woodbury (2015a) proposed the use of artificial neural network for near real-time heat flux estimation in a two-dimensional problem based on the idea of digital filter coefficients. Prasad et al. (2017) proposed a real time tool monitoring using the combination of multiple sensors signals including temperature and vibration. Han et al. (2020) developed a pyrometer system to obtain the real-time cutting temperature in turning process of difficult-to-cut material. It was found that the cutting temperature rises sharply before the tool breakage.

In the current paper, an Al2O3-TiC ceramic tool was used to cut a workpiece of nodular cast iron while a thermal imaging camera was performing temperature measurements. It was proposed a filter coefficient solution in a nonlinear three-dimensional model to solve the IHCP in real time. Furthermore, a methodology was developed to estimate the hottest temperature.

2. MODEL DESCRIPTION

The thermal model used in this work is shown in figure 1. The assembly consists of a ceramic insert, tool holder, screw and shim.

The heat-flux, (t) , entering the tool-chip interface is considered uniformly distributed over this area. In Fig. 1 the tool-chip interface is denoted as S_1 and there is a convective cooling on the major flank face, S_2, due to an air jet acting parallel to this surface. The remaining surfaces are subjected to natural convection and the radiation heat loss to the surroundings is also considered.

The thermal model of the assembly shown in Fig. 1 may be described by the nonlinear transient three-dimensional heat diffusion equation:

$$\frac{\partial}{\partial x}\left(k\left(T\right)\frac{\partial T}{\partial x}\right)+\frac{\partial}{\partial y}\left(k\left(T\right)\frac{\partial T}{\partial y}\right)+\frac{\partial}{\partial z}\left(k\left(T\right)\frac{\partial T}{\partial z}\right)=\rho c\left(T\right)\frac{\partial T}{\partial t} \tag{1}$$

where T is the temperature, x, y, and z the Cartesian coordinates, ρ the density, t is the time and $k(T)$ and $c(T)$ are the temperature dependent thermal conductivity and specific heat, respectively.

The heat flux boundary condition at the tool-chip interface is given by:

$$-k\left(T\right)\frac{\partial T}{\partial z}=q\left(t\right),\quad \text{on } S_1 \tag{2}$$

For all the surfaces exposed to the ambient air the boundary conditions of convection and radiation are considered:

$$-k\left(T\right)\frac{\partial T}{\partial \eta}=h\left(T-T_\infty\right)+\sigma\varepsilon\left(T\right)\left(T^4-T_\infty^4\right) \tag{3}$$

where η is the normal direction, h the heat transfer coefficient, σ the Stefan-Boltzmann constant, ε the emissivity and T_∞ is the ambient temperature.

The boundary condition for the surface subjected to the air jet is:

$$-k\left(T\right)\frac{\partial T}{\partial \eta}=\bar{h}_f\left(T\right)\left(T-T_\infty\right),\quad \text{on } S_2 \tag{4}$$

where $\bar{h}_f$ is the average heat transfer coefficient. It may be calculated from the empirical correlation defined by Bergman et al. (2017) as:

$$\bar{h}_f = 2\frac{k_f}{L}\frac{0.3387\,\mathrm{Pr}^{1/3}\,\mathrm{Re}_L^{1/2}}{\left(1+\left(\frac{0.0468}{\mathrm{Pr}}\right)^{2/3}\right)^{1/4}}, \quad \mathrm{Re}_L \le 5\times10^5 \tag{5}$$

where k_f is the thermal conductivity of the fluid, L the plate length, Pr the Prandtl number and Re_L the Reynolds number.

The initial condition is:

$$T(x,y,z,0) = T_\infty \tag{6}$$

3. INVERSE PROBLEM

In this section, the methodology used to solve the inverse heat conduction problem in real time in a machining process using a ceramic cutting tool is presented and discussed. This problem consists of estimating the heat flux at the tip-tool interface during machining by measuring the temperature on access positions on the cutting tool surface using an IR camera. Once the heat flux is obtained, it is possible to estimate the hot spot temperature of the cutting tool in real time as well. To make the heat flux estimation possible in real time, a methodology based on filter solutions proposed by Beck (2008) and the classical Function Specification Method (Beck et al., 1985) was used.

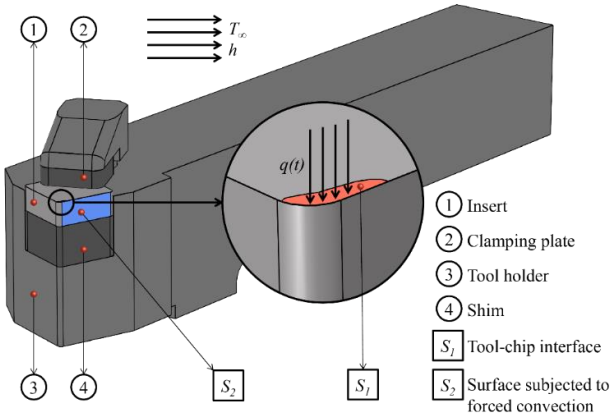

Figure 1. Insert-tool holder assembly with thermal model and boundary conditions.

3.1 The filter solution method

Considering Y the measured temperature at an internal point of the domain, $\hat{q}$ the estimated heat flux and g the filter coefficient, the filter solution to the time step M is given by

$$q_M = \sum_{j=1}^{m_p+m_f} g_j Y_{m_f+M-j}, \quad M = m_p+1, m_p+2, \ldots \tag{7}$$

where m_p and m_f are the number of past and future times associated with the measured temperatures in relation to time M. In order to facilitate the computational implementation, Eq. (7) can be rewritten in a matrix form as shown in Eqs. (8) and (9).

$$q_M = \mathbf{g}_f^{\mathrm{T}}\mathbf{Y}_f + \mathbf{g}_p^{\mathrm{T}}\mathbf{Y}_p \tag{8}$$

$$\mathbf{g}_f = \begin{bmatrix} g_1 \\ g_2 \\ \vdots \\ g_{m_f} \end{bmatrix} \mathbf{g}_p = \begin{bmatrix} g_{m_p} \\ g_{m_p+1} \\ \vdots \\ g_{m_p+m_f} \end{bmatrix} \mathbf{Y}_f = \begin{bmatrix} Y_{M+m_f-1} \\ Y_{M+m_f-2} \\ \vdots \\ Y_M \end{bmatrix} \mathbf{Y}_p = \begin{bmatrix} Y_{M-1} \\ Y_{M-2} \\ \vdots \\ Y_{M-m_p} \end{bmatrix} \tag{9}$$

As shown in Eq. (7), the objective of the filter solution is to directly calculate the heat flux using only temperature data near the time M and the filter coefficients. Thus, with the simplicity of the calculation and the capability to obtain results sequentially, the filter solution makes it possible to estimate the heat flux in real time.

Some observations should be noted in Eqs. (7) and (8). First, the filter coefficients are independent of the time t_M and the experimental temperatures, so they need to be calculated only once for a given case. In addition, the filter coefficients may be used for any measurement time interval for the same problem. Second, heat flux values are lost in time steps of less than $m_p + 1$. A basic solution to this problem is to perform $m_p + 1$ temperature measurements while the material is at the initial temperature T_0, or add $m_p + 1$ components to the beginning of the experimental temperature vector, **Y**. This last strategy is recommended for scenarios in which the value of past times is large.

To calculate the filter coefficients, it is necessary to use some inverse problem with regularization. The most commons techniques are the Tikhonov Regularization method (Najafi et al., 2015b), (Beck, 2008), (Woodbury and Beck, 2013) and (Uyanna and Najafi, 2019) and the Sequential Function Specification Method (SFMS) (Beck, 2008) and (Blackwell and Beck, 2010). In this work, SFSM was employed because of its robustness and ease of implementation.

The SFSM algorithm for one temperature sensor is described by Eq. (10). More detail about the method can be found in Beck et al. (1985).

$$q_M = \frac{\sum_{i=1}^{r}\left(Y_{M+i-1} - T_{M+i-1}\Big|_{q_M = q_{M+1} = \ldots = 0}\right)\varphi_i}{\sum_{i=1}^{r}\varphi_i^2} \tag{10}$$

In Eq. (10), r is the number of future time steps and φ represents the thermal sensitivity in a point at the domain for a given problem. The estimated temperatures, $\hat{T}$, are calculated with an approximation of the Duhamel's theorem as shown in Eqs. (11) and (12).

$$T_{M+i-1} = T_0 + \sum_{n=1}^{M-1} q_n \Delta\varphi_{M-n+r-1} \tag{11}$$

$$\Delta\varphi_i = \varphi_{i+1} - \varphi_i \tag{12}$$

Since machining is considered a nonlinear problem, the sensitivity coefficients should be calculated numerically in order to solve the partial derivative $\partial T/\partial q$ at time t_i and position r in the three-dimensional domain.

$$\varphi(\mathbf{r}, t_i) = \varphi_i = \frac{T\left(\mathbf{r}, (1+\delta)q_i\right) - T(q_i)}{\delta q_i}, \quad \delta << 1 \tag{13}$$

To calculate the filter coefficients, **g**, one must first obtain the thermal sensitivities using Eq. (13). Then, a value will be selected for the number of future times r. Next, the vector of experimental temperatures **Y** must be made null, except for the coordinate r, as shown in Eq. (14).

$$\begin{aligned} Y_i &= 0, \quad i = 1, 2, \ldots, r-1, r+1, \ldots, N \\ Y_r &= 1 \end{aligned} \tag{14}$$

The heat flux vector $\hat{\mathbf{q}}$ should be found using Eq. (10). Thus, the vector of the filter coefficients is given by $\mathbf{g} = \hat{\mathbf{q}}$. It is important to know that the number of future time steps has influence in the filter coefficient values along with the thermal sensitivity. In this way, it is necessary to carefully choose the parameter through simulated cases with the same geometry and properties as the real scenario. In addition, just like the thermal sensitivity, the filter coefficients depend on temperature in nonlinear cases. A solution to this problem is to calculate the filter coefficients for discrete temperature values in a given interval and save them in a database that can be accessed in real time according to the temperatures that are measured in the process. This is an approximate technique that was proposed by Beck (2008) and allows the interpolation of the filter coefficients during the solution in real time and is used in this article.

3.2 Accuracy of heat flux estimation

In general, temperature sensors located far from the heat flux boundary condition and low thermal conductivity materials decrease the IHCP solution accuracy. Recent articles involving filter solutions apply the method proposed here, generally in one-dimensional geometries and favorable situations for estimating heat flux. In real applications, the conditions available to solve the problem are often not the best, as is the case studied in this article. In this case, the formation of chips on the cutting edge of the tool prevents the visualization of a measurement point very close to the heat flux area by the IR camera. In addition, the heat distribution is three-dimensional and the ceramic tool has low thermal conductivity. Thus, it is important to establish parameters that can measure how accurate the heat flow estimation is and, if possible, correct systematic errors.

With $\mathbf{q}$ being the true heat flux value and $\hat{\mathbf{q}} = \mathbf{gY}$ the estimated heat flux, the residual sum of squares in the errors in the estimation is given by

$$R_q = \left(\mathbf{q}-\mathbf{q}\right)^{\mathrm{T}}\left(\mathbf{q}-\mathbf{q}\right) = \left(\mathbf{gY}-\mathbf{q}\right)^{\mathrm{T}}\left(\mathbf{gY}-\mathbf{q}\right) \tag{15}$$

Thus, the expected value of R_q is

$$E\left(R_q\right) = E\left[\left(\mathbf{gY}\right)^{\mathrm{T}}\mathbf{gY}\right] - \left[\mathbf{g}E\left(\mathbf{Y}\right)\right]^{\mathrm{T}}\mathbf{q} - \mathbf{q}^{\mathrm{T}}\mathbf{g}E\left(\mathbf{Y}\right) + \mathbf{q}^{\mathrm{T}}\mathbf{q} \tag{16}$$

As shown in the Appendix of Woodbury and Beck (2013), the expected value consists of two parts:

$$E\left(R_q\right) = E_{bias} + E_{rand} \tag{17}$$

$$E_{bias} = \mathbf{q}^{\mathrm{T}}\left(\mathbf{P}-\mathbf{I}\right)^{\mathrm{T}}\left(\mathbf{P}-\mathbf{I}\right)\mathbf{q} \tag{18}$$

$$E_{rand} = \sigma_Y^2 tr\left(\mathbf{g}^{\mathrm{T}}\mathbf{g}\right) \tag{19}$$

where $\mathbf{P} = \mathbf{gX}$, being $\mathbf{X}$ the sensitivity matrix.

It can be noted that the portion referring to the bias depends on the matrix $\mathbf{P}$ and the heat flux $\mathbf{q}$, while the component of random errors depends on the variance of the temperature measurement errors.

As discussed in Beck and Woodbury (2016), the $\mathbf{P}$ matrix is a great indicator of the quality of the solution to the inverse problem. For cases in which the heat flux is constant, $\mathbf{P}$ is approximately symmetric and the sum of the elements in a column is close to 1 while the bias value is nearly zero. This is an important result for the problem studied in this article since the heat flux in machining remains approximately constant over the cutting time.

3.3 Estimated temperature at the cutting edge

Since the estimated heat flux is known, it is possible to calculate the temperatures on the cutting region of the tool. With g_{hs} being the filter coefficients at the hot spot location, the heat flux in the process is given by

$$q_M = \mathbf{g}_{hs_f}^{\mathrm{T}}\mathbf{T}_{hs_f} + \mathbf{g}_{hs_p}^{\mathrm{T}}\mathbf{T}_{hs_p} \tag{20}$$

where T_{hs} is the temperature of the hot spot. Considering that the temperatures of past times, Y_{hs_p} are known, it is possible to use an approach similar to SFSM to estimate the temperature at the current time t_M. For this purpose, a temporary constant function form for the temperature from time t_M to t_{M+m_f-1} is assumed, as shown in Eq. (21).

$$T_{hs_M} = T_{hs_{M+1}} = T_{hs_{M+2}} = \cdots = T_{hs_{M+m_f-1}} \tag{21}$$

Substituting $q_M = \hat{q}_M$ and Eq. (21) in Eq. (20), the hot spot temperature at time t_M is calculated by

$$T_{hs_M} = \frac{q_M - \mathbf{g}_{hs_p}\mathbf{Y}_{hs_p}}{\sum_{i=1}^{m_f} g_{hs_{M+i-1}}} \tag{22}$$

The summation in the denominator of Eq. (22) behaves as a regularization term to estimate accurate values of the hot spot temperature. If m_f is low, a large oscillatory behavior may occur at the beginning of estimation.

4. EXPERIMENTAL PROCEDURE

In this work, the temperature field during the oblique turning process with air cooling was investigated. The machining tests were carried out in a conventional lathe NARDINI Logic 175. The material used was a cylindrical nodular cast iron GGG40 bar of 50 mm diameter and 135 mm length. The tool holder of AISI 4340 steel (BT25-CSRNR-2540-12-IC) the carbide shim and the carbide clamp were employed to hold the ceramic insert (ISO SNGN 120408 T01020 CC650). In order to measure the temperature field, a thermal camera FLIR T450sc was used.

To minimize the chip influence on the temperature field measured by the thermal camera, 6-bar compressed air with a velocity of 30 m/s was applied parallel in one face of the insert. The pressure was measured using a manometer and the air velocity was measured using an anemometer model testo 445.

A total of four tests (E1, E2, E3 and E4) were conducted. The first three tests were used to obtain the average contact surface. In the last test E4 the thermal camera with the software was employed to obtain the thermal field in the insert in real time. The feed rate of 0.2 mm/rot, depth of cut of 1.5 mm, cutting speed of 150 m/min and machining length of 65 mm were fixed parameters for all experiments.

5. NUMERICAL MODEL

5.1 Thermal properties and mesh

The direct problem described in Section 2 was solved by the Finite Element Method by using COMSOL Multiphysics 5.5 software. Table 1 shows the parameter values of the thermal model. The thermal properties of each material were considered dependent on temperature with the exception of density. Figure 2 and Fig. 3 presents the thermal properties used to calculate the temperature field in the direct problem. The properties of AISI 4340 and Tungsten Carbide (WC) steel were obtained from Fakir et al. (2018) and Jiang et al. (2016), respectively. The thermal conductivity and specific heat of the ceramic tool (Al_2O_3-TiC) were experimentally obtained using the flash method by Bhusan (1987). In this work, a cubic extrapolation for thermal conductivity and linear extrapolation for the specific heat was used in order to obtain an approximation to the thermal properties at high temperatures on the chip-tool interface.

The tetrahedral mesh was obtained through a mesh convergence study, Fig. 4. Four mesh configurations M1, M2, M3 and M4 with 10255, 17764, 40857, 107009 elements, respectively, were considered. The average temperature difference between the meshes was used as a convergence criterion. Thus, it was admitted that the convergence was obtained in the M4 mesh with an average temperature difference of 0.09 °C.

Table 1. Thermal model parameters.

Parameter	Value	Description
h	10 W/(m^{2}K)	Natural convection coefficient
U	30 m/s	Fluid velocity
p_a	1.6 atm	Absolute pressure
L	12.7 mm	Plate length
ε_{WC}	0.8	Emissivity of tungsten carbide
ε_c	0.9	Ceramic tool emissivity
ε_s	0.85	Emissivity of AISI 4340 steel
ρ_{WC}	14100 kg/m^3	Density of tungsten carbide
ρ_c	4220 kg/m^3	Ceramic tool density
ρ_s	7870 kg/m^3	Density of AISI 4340 steel
T_0	22.0 °C	Room temperature

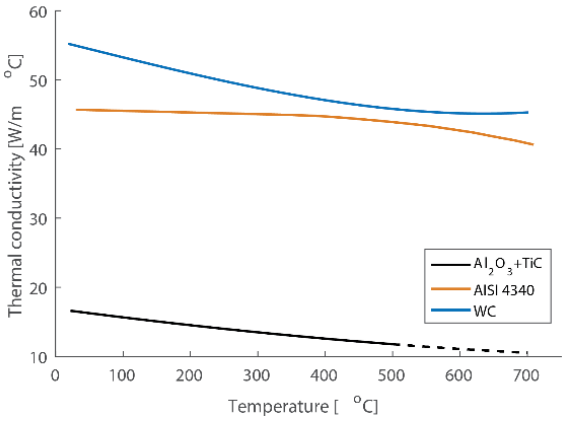

Figure 2. Thermal conductivities of the materials.

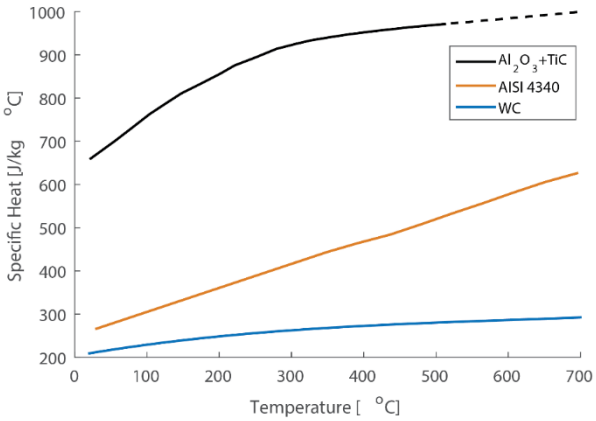

Figure 3. Specific heats of the materials.

5.2 Determination of the heat flux area

The heat flux boundary condition area in the rake face caused by the contact between the chip and the tool varies slightly between experiments using the same depth of cut. Although this variation is small, this fact makes it difficult to estimate the heat flux in real time since the true area of heat flux will always be unknown from one machining process to another. To minimize this problem, a methodology is proposed to determine an average curve that delimits the heat flux area on the rake face of the tool. For this, the profiles of the measured areas in previous experiments (E1, E2 and E3) are used as data.

This work uses the definition of average curve based on zAC (Zero-set Average Curve) proposed by Sati et al. (2016). The obtained curve was used for the real time estimation.

6. RESULTS AND DISCUSSION

Three cases were studied in order to validate the inverse problem methodology described in Section 3. The simulated heat fluxes for cases 1, 2 and 3 are 7×10^6, 9×10^6 and 2×10^7 W/m^2, respectively. These values represent the order of magnitude of a heat flux generated. In this way, the simulated temperature in the measurement coordinate $(5.9, 1.6, 0)$ mm was calculated. In order to simulate the measurement in real time, a function was created in the program to read a temperature from the vector of experimental temperatures at each time interval of 0.033 s.

Figure 5 shows the sensitivity coefficients, φ, as function of time at temperatures of $22.1\,°C$ (room temperature), $250\,°C$, $500\,°C$ and $750\,°C$. As mentioned in Section 3.1, the nonlinearity of the problem requires that the filter coefficients are calculated as a function of temperature (Fig. 6) and interpolated during the calculation of the heat flux.

From time step 2000 onwards, the filter coefficients reach values approximately constant and close to zero. Therefore, to ensure a good heat flux estimation, $m_f + m_p = 2000$ was used with $m_f = 26$ future times steps. To avoid the delay of m_p initial temperature measurements, a vector of size m_p is created before starting the estimation with its components equal to the initial temperature.

In order to simulate the measurement in real time, a function was created to read the vector of simulated temperatures at a rate of 30 Hz.

The temperature at the hot spot was calculated using Eq. (21). A comparison between the estimated and the exact temperature, which was calculated by the direct problem with the true heat flux, is shown in Fig. 7. It can be noted that the exact values are well represented by the estimated ones, once the residuals are close to zero. The residuals are higher when there is a sudden change in temperature, which commonly occurs in techniques with regularization in step function.

In order to apply the methodology to monitor the heat flux and the hot spot temperature in a machining process the software ”Real Time Heat Flux Monitor” was implemented. It was developed in order to control a FLIR camera and link it to the inverse problem solver. The software has a Graphical User Interface (GUI) where the user is able to visualize in real time measured temperature data and the estimated values of the heat flux and the temperature at the hot spot, as well as choose the future time step parameter and follow the machining through live video recording.

The E4 experiment was performed in order to apply the methodology in a real machining process. The numerical model described in Section 5 was used, in which the heat flux boundary area was calculated by zAC (section 5.2).

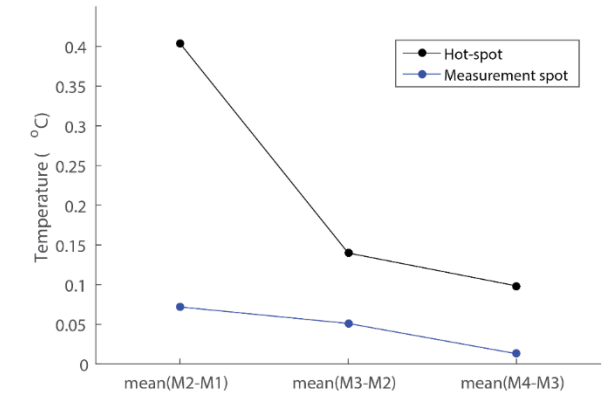

Figure 4. Details of the mesh convergence study.

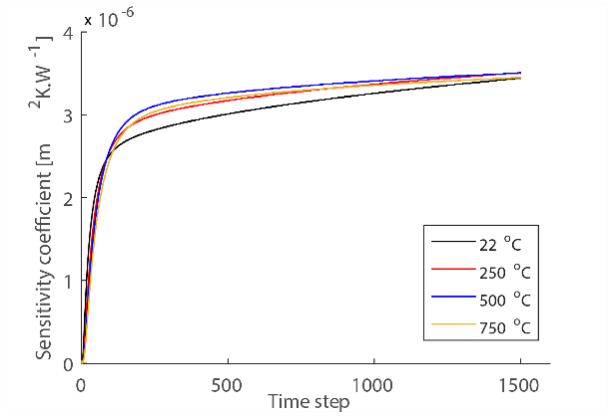

Figure 5. Sensitivity coefficients.

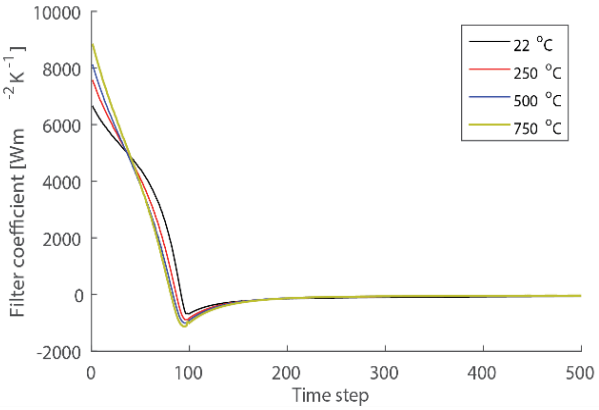

Figure 6. Filter coefficients.

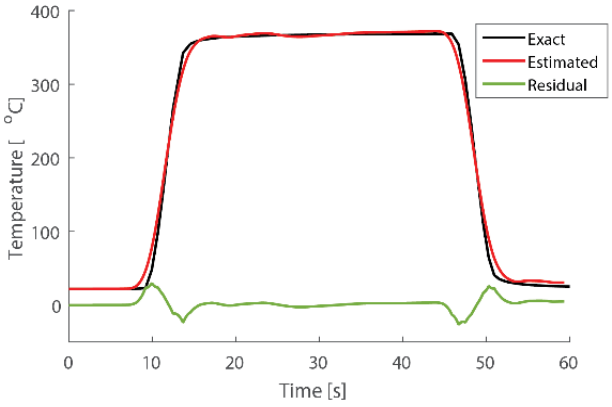

Figure 7. Comparison between the exact and estimated temperatures in the hot spot.

Figure 8 shows the temperature data in red, measured by the IR camera during the machining process in coordinates $(5.9, 1.6, 0)$ mm on the rake face of the tool. It can be noted that there are spikes all over the experimental curve due to the chips passing between the measurement point and the camera. This fact is a problem to the estimation since the IHCP is very sensitive to the input data. Thus, a solution is to smooth the data over time as shown in Fig. 8. However, it will cause an increase in computational time, adding some delay to the estimation procedure. In this problem, the lowess method (locally weighted scatter-plot smooth) was used to smooth the data over time considering the previous 100 points of measured temperatures in relation to the current time step. In addition, according to the manufacturer, the uncertainty of the IR camera is 2%, which represents 1.14 °C based on the maximum smoothed temperature.

The real-time estimated heat flux using the area bounded by zAC is shown in Fig. 9. In Fig. 9 it can also be seen the heat flux estimated offline. The offline estimation was calculated using the classical SFSM method (Beck et al., 1985) and (Woodbury, 2002). The two results present the same behavior and their values are very close with an average error of 2.99% in relation to the offline estimation. For this machining process the estimated heat flux reached a maximum of 1.41×10^7 W/m^2, remaining in a steady state of approximately 1.38×10^7 W/m^2; after 30 s. It can be noted that there are no large fluctuations in the estimated heat flux due to the smoothing of the temperature data over time.

The real time estimated temperature at the hot spot is shown in Fig. 10. In order to verify the method accuracy, a comparison was made in relation to the calculated temperatures using the offline estimated heat flux. Both methods have practically the same results, except by the large oscillation at the beginning of the real-time estimation ($t = 10$ s). Note that this fluctuation is caused by the small number of future times, $m_f = 26$, used in the estimation. A larger value of m_f can smoothen the transition. The minimum value of m_f in the heat flux estimation should be determined by the quality of the temperature estimation. The residuals in the stable phase are very low in comparison to the estimated temperature, as shown in Fig. 11. The mean of residuals is 6.76 °C, which represents 0.95% of the maximum temperature.

An error in the estimated heat flux causes an even smaller error in the estimated temperature. In this way, small variations in the heat flux boundary condition area will not have much influence on the temperature result at the hot spot.

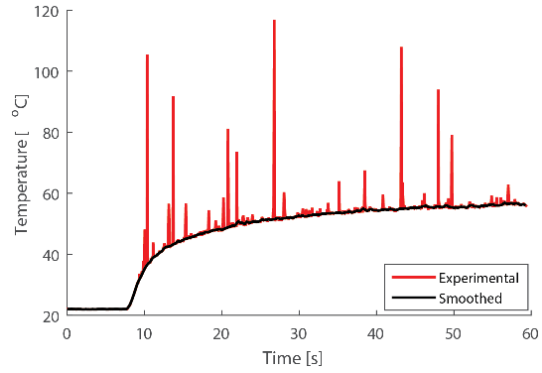

Figure 8. IR smoothed curve used in computation.

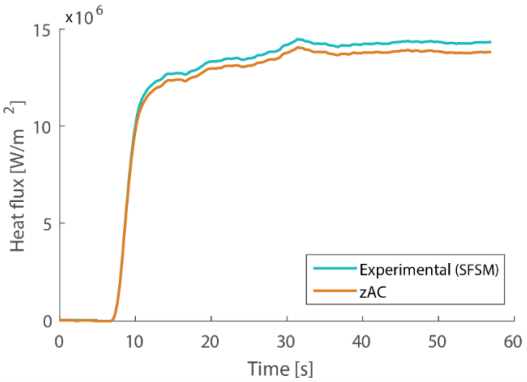

Figure 9. Real time and offline estimated heat flux.

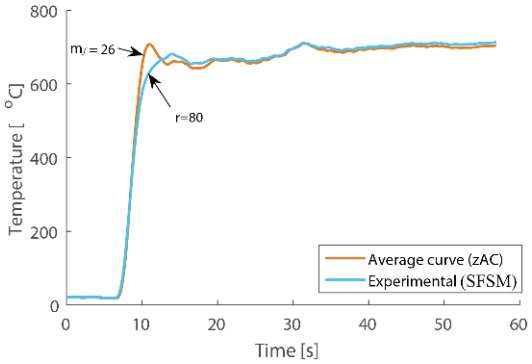

Figure 10. Real-time and offline estimated temperature on the hotspot.

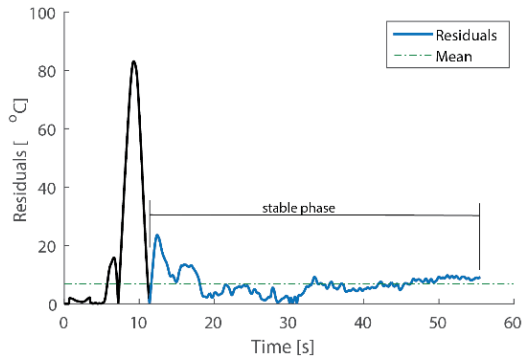

Figure 11. Residuals for the real-time estimated temperature on the hot spot.

7. CONCLUSION

In this paper, a complete methodology to online estimate simultaneously the heat flux and the hot spot temperature in a machining process using a filter coefficients approach is presented. Instead of using thermocouples to measure temperature data, an IR camera was used since it is not possible to attach thermocouples on the ceramic tool by welding.

In order to test the methodology with real data, a machining experiment was performed. It can be said that the filter coefficients method can estimate heat flux very well with step function behavior, which is the case for machining (Dourado et al., 2021). A comparison was made between the online and offline estimated heat flux using two different approaches (filter coefficient and SFSM). The results are very similar, diverging only because the real area of the heat flux boundary condition is slightly different from the area obtained by zAC. On the other hand, there was almost no difference between the estimated temperatures at the hot spot, with the mean of residuals of 6.76 °C.

As a result of this work, a computational software (Real Time Heat Flux Monitor) was developed to facilitate the monitoring of heat flux and temperature in machining process. It can also be used to monitor other processes in which it is difficult or impossible to measure these parameters.

8. ACKNOWLEDGEMENTS

The authors would like to thank the Brazilian sponsors CNPq, CAPES and FAPEMIG for their financial support.

9. REFERENCES

Abukhshim N.A., Mativenga P.T. and Sheikh M.A., 2005. “Investigation of heat partition in high speed turning of high strength alloy steel”. *Int. J. Mach. Tool Manufact.*, Vol. 45, pp. 1687–95.

Abukhshim N.A., Mativenga P.T. and Sheikh M.A., 2006. “Heat generation and temperature prediction in metal cutting: a review and implications for high speed machining”. *Int. J. Mach. Tool Manufact.*, Vol. 46, pp. 782–800.

Arrazola P.J., Özel T., Umbrello D., Davies M. and Jawahir I.S., 2013. “Recent advances in modelling of metal machining processes”. *CIRP Annals*, Vol. 62, pp. 695–718.

Beck J.V., Jr S.C., Blackwell B., Clair C.R.S. and Clair C.R.S., 1985. *Inverse Heat Conduction: Ill-Posed Problems*. Wiley-Interscience publication, Wiley.

Beck J.V., 2008. "Filter solutions for the nonlinear inverse heat conduction problem". *Inverse Probl Sci Eng.*, Vol. 16, pp. 3–20.

Beck J.V. and Woodbury K.A., 2016. "Inverse heat conduction problem: sensitivity coefficient insights, filter coefficients, and intrinsic verification". *Int. J. Heat Mass Tran.*, Vol. 97, pp. 578–588.

Bergman T.L., Lavine A.S., Incropera F.P. and DeWitt D.P., 2017. *Fundamentals of Heat and Mass Transfer*. Wiley.

Bhushan B., 1987. "Magnetic head-media interface temperatures: Part 2 application to magnetic Tapes". *Tribol.*, Vol. 109, pp. 252–6.

Blackwell B. and Beck J.V., 2010. "A technique for uncertainty analysis for inverse heat conduction problems". *Int. J. Heat Mass Tran.*,Vol. 53, pp. 753–9.

Carvalho S.R., Lima e Silva S.M.M., Machado A.R. and Guimarães G., 2006. "Temperature determination at the chip–tool interface using an inverse thermal model considering the tool and tool holder". *Mater. Process. Technol.*, Vol. 179, pp. 97–104.

Dourado da Silva R.G., Ferreira D.C., Dutra F.V.A. and Lima e Silva S.M.M., 2021. "Simultaneous real time estimation of heat flux and hot spot temperature in machining process using infrared camera". *Case Stud. Therm. Eng.*, Vol. 28, pp. 101352.

Fakir R., Barka N. and Brousseau J., 2018. "Case study of laser hardening process applied to 4340 steel cylindrical specimens using simulation and experimental validation". *Case Stud. Therm. Eng.*, Vol. 11, pp. 15–25.

Grzesik W. and Nieslony P., 2003. "A computational approach to evaluate temperature and heat partition in machining with multilayer coated tools". *Int. J. Mach. Tool Manufact.*, Vol. 43, pp. 1311–17.

Han J., Cao K., Xiao L., Tan X., Li T., Xu L., Tang Z., Liao G. and Shi T., 2020. "In situ measurement of cutting edge temperature in turning using a near-infrared fiber-optic two-color pyrometer". *Measurement*, Vol. 156, pp. 107595.

Heigel J.C., Whitenton E., Lane B., Donmez M.A., Madhavan V. and Moscoso-Kingsley W., 2017. "Infrared measurement of the temperature at the tool–chip interface while machining Ti–6Al–4V". *J. Mater. Process. Technol.*, Vol. 243, pp. 123–130.

Jiang F., Zhang T. and Yan L., 2016. "Estimation of temperature-dependent heat transfer coefficients in near-dry cutting". *Int. J. Adv. Manuf. Technol.*, Vol. 86, pp. 1207–1218.

Le Coz G., Marinescu M., Devillez A., Dudzinski D. and Velnom L., 2012. "Measuring temperature of rotating cutting tools: application to mql drilling and dry milling of aerospace alloys". *Appl. Therm. Eng.* Vol. 36, pp. 434–441.

Liang L., Xu H. and Ke Z., 2013. "An improved three-dimensional inverse heat conduction procedure to determine the tool-chip interface temperature in dry turning". *Int. J. Therm. Sci.*, Vol. 64, pp. 152–161.

Najafi H and Woodbury K A 2015a Online heat flux estimation using artificial neural network as a digital filter approach". *Int. J. Heat Mass Tran.*, Vol. 91, pp. 808–817.

Najafi H., Woodbury K.A. and Beck J.V., 2015b. "Real time solution for inverse heat conduction problems in a two-dimensional plate with multiple heat fluxes at the surface". *Int. J. Heat Mass Tran.*, Vol. 91, pp. 1148–1156.

Prasad B.S., Prabha K.A. and Kumar P.V.S.G., 2017. "Condition monitoring of turning process using infrared thermography technique – an experimental approach". *Infrared Phys. Technol.*, Vol. 81, pp. 137–147.

Rezende B.A., Magalhães F.C. and Campos Rubio J.C., 2020. "Study of the measurement and mathematical modelling of temperature in turning by means equivalent thermal conductivity". *Measurement*, Vol. 152, pp. 107275.

Sati M., Rossignac J., Seidel R., Wyvill B. and Musuvathy S., 2016. "Average curve of n smooth planar curves". *Comput Aided Des.*, Vol. 70, pp. 46–55.

Sheikh-Ahmad J.Y., Almaskari F., Hafeez F. and Meng F., 2019. "Evaluation of heat partition in machining cfrp using inverse method". *Mach. Sci. Technol.*, Vol. 23, pp. 530–546.

Soler D., Aristimuño P., Saez-de Buruaga M. and Arrazola P., 2018. "New calibration method to measure rake face temperature of the tool during dry orthogonal cutting using thermography". *Appl. Therm. Eng.*, Vol. 137, pp. 74–82.

Uyanna O. and Najafi H., 2019. "A near real-time solution approach for surface heat flux estimation in one dimensional inverse heat conduction problems with moving boundary". ASME 2019 Heat Transfer Summer Conf., p. 8.

Valiorgue F., Brosse A., Naisson P., Rech J., Hamdi H. and Bergheau J.M., 2013. "Emissivity calibration for temperatures measurement using thermography in the context of machining". *Appl. Therm. Eng.*, Vol. 58, pp. 321–6.

Woodbury K.A., 2002. *Inverse Engineering Handbook*. CRC Press, 1st edition.

Woodbury K.A. and Beck J.V., 2013. "Estimation metrics and optimal regularization in a Tikhonov digital filter for the inverse heat conduction problem". *Int. J. Heat Mass Tran.*, Vol. 62, pp. 31–39.

10. RESPONSIBILITY NOTICE

The authors are the only responsible for the printed material included in this paper.